Journal of Molecular Liquids 366 (2022) 120230

Contents lists available at ScienceDirect

Journal of Molecular Liquids

journal homepage: www.elsevier.com/locate/molliq

On the structure and stability of novel cationic DPPC liposomes doped with gemini surfactants

Vicente Domínguez-Arca [a,*], Juan Sabín [a,b], Luís García-Río [c], Margarida Bastos [d], Pablo Taboada [e,f], Silvia Barbosa [e,f], Gerardo Prieto [a,f,*]

[a] Grupo de Biofísica e Interfases, Departamento de Física Aplicada, Facultad de Física, Universidad de Santiago de Compostela, 15782 Santiago de Compostela, Spain
[b] AFFINImeter-Software 4 Science Developments, S.L. Edificio Emprendia s/n, Campus Vida, Santiago de Compostela, Spain
[c] Departamento de Química Física, Facultad de Quimica, Universidad de Santiago, 15782 Santiago. Spain
[d] CIQ-UP, Institute of Molecular Sciences (IMS), Departamento de Química e Bioquímica, Faculdade de Ciências da Universidade do Porto, R. Campo Alegre 687, P-4169-007 Porto, Portugal
[e] Grupo de Física de Coloides y Polímeros, Departamento de Física de Partículas, Universidad de Santiago de Compostela, 15782-Santiago de Compostela, Spain
[f] Instituto de Materiales, Universidad de Santiago de Compostela, E-15782 Santiago de Compostela, Spain

ARTICLE INFO

Article history:
Received 22 March 2022
Revised 24 August 2022
Accepted 26 August 2022
Available online 30 August 2022

Keywords:
Gemini surfactants
Cationic liposomes
Trans-gauche isomerization
Lambda transitions
Lipid-surfactant interactions

ABSTRACT

A novel formulation of cationic liposomes was studied by mixing dipalmitoylphosphatidylcholine (DPPC) with tetradecyltrimethylammonium bromide gemini surfactants with different alkane spacer groups lengths attached to their ammonium head-groups. The physicochemical characterization of the cationic liposomes was obtained by combining experimental results from differential scanning microcalorimetry (DSC) with molecular dynamic simulations, in order to understand their structural configuration. An adapted Ising model was used to interpret the results in terms of cooperativity of the phase transitions.

The gemini surfactants partition into the lipid bilayer of DPPC liposomes, and the induced changes in colloidal stability and phase transition were analyzed in detail. The DPPC liposomes became positively charged upon gemini surfactant partition, showing increased colloidal stability. Our results show significant differences in structural configuration between gemini surfactants with short and long spacer lengths. While gemini with shorter spacers allocate within the lipid bilayer with both headgroups in the same layer, geminis with longer spacers unexpectedly intercalate in the lipid membrane in a particular zig-zag configuration, with each headgroup located at a different side of the bilayer, altering the coupling degree parameters of the membrane's phase transition.

The extraordinary increase of colloidal stability of DPPC liposomes with gemini surfactants at very low molar ratio and the possibility to tune the physicochemical properties of the membrane by control de spacer length of the geminis opens new possibilities for cationic liposomal formulations with potential applications in vaccines, drug/gene delivery or biosensing.

1. Introduction

The nature and physical properties of different classes of nanoparticles (NPs) offers possibilities to encapsulate and transport molecular bioactive cargoes, functionalize surfaces or build new biosensors[1]. From the first works reporting their synthesis, characterization, and potential biomedical applications [2], liposomes became a key player in nanoparticle pharmaceutical technology. They are structures formed by the dispersion of lipids in aqueous media, commonly in the form of closed lipid bilayers with an inner aqueous core. The basic structure of liposomes can be seen as a very simple model of the cell membrane, and that has been largely explored in the use liposomes as natural-based nanocarriers for drug loading [34], or as biomimetic models[5] of more complex biological systems. NPs for potential clinical applications as gene therapy, drug delivery or vaccines must have colloidal stability in physiological media [6] and positive surface charge for better interaction with target cells. The non-availability of natural cationic lipids implies the need to explore liposome formulations with cationic synthetic molecules, such as double-chained quaternary ammonium[7,8] or cationic single-chained surfactants[9].

* Corresponding authors at: Grupo de Biofísica e Interfases, Departamento de Física Aplicada, Facultad de Física, Universidad de Santiago de Compostela, 15782 Santiago de Compostela, Spain (G. Prieto).
E-mail addresses: vicente.domarc@gmail.com (V. Domínguez-Arca), xerardo.prieto@usc.es (G. Prieto).

https://doi.org/10.1016/j.molliq.2022.120230
0167-7322/

The presence of cationic lipids/surfactants in liposome formulations gives rise to changes in the conformation of the resulting lipid bilayer and, as a consequence, in the NP colloidal stability[7,10] and/or biocompatibility[11]. The clever choice of suitable molecular species and lipid/surfactant molar ratios are the key for a successful synthesis of cationic liposomes. Following previously reported works[7,12–14], the strategy to obtain cationic liposomes from DPPC bilayers can be based on the use of gemini surfactants as liposome cationic additives. We used gemini surfactants having an hydrocarbon linkage between quaternary ammonium salts, synthesized as described in Materials and Methods Although the strategy for using these liposome formulations is known, the details about their location and consequent implications in the lipid bilayer structure and function remain unclear. The aim of present work was to shed light on the effect of the gemini surfactant on the structure and stability of the DPPC liposomes, this aim as well as the approach taken (DSC and MD study) represent the novelty of our work. These amphiphiles have been used in other biophysical applications[15–19] such as membrane solubilization or in the design of non-viral gene vectors due to their low toxicity [20]. They can also be found in different industrial processes as emulsifiers, dispersants, coating agents, or corrosion inhibitors [21,22]. Gemini surfactants show a higher surface activity[23], lower critical micelle concentrations (CMCs) and Kraft temperatures, when compared with their single-chain counterparts[24,25]. They can assume different morphological structures[26,27] such as vesicles, helices, or tubules, in different lyotropic phases.

The partition of gemini surfactants to the liposomes changes the morphology and structure of the lipid bilayer, altering the membrane phase transitions. These phase transitions are commonly studied assuming a simple two-state (gel/fluid) model[28], cooperativity theories[29] or simulated by Montecarlo methodologies[30]. In this work, we use a theoretical framework based on the transcendent physical paradigm of the Ising model for the interpretation of the role of gemini surfactants on the phase transitions in lipid bilayers. The Ising model is a statistical mechanics model that has been traditionally used to explain ferromagnetism and other temperature-dependent phase transitions[31]. In general terms, the conventional Ising model for phase transitions describes a bi-dimensional lattice with nodes which are occupied by a particle with two possible states (+1 or −1). Each particle is coupled at least with the first neighbours, i.e., the state of the ith-particle is influenced by its first neighbours. Under these hypotheses, a critical temperature exists below which all particles will have the same state. Therefore, the homogeneous 2D Ising model, if successfully applied to lipid bilayers systems[32], might help in understanding the factors that play a key role on the phase transition, and how this transition and its characteristic temperature change when lipid bilayers are doped with surfactants. 2D Ising model takes the following mathematical form of its Hamiltonian (in the absence of an external field): $H = J \Sigma s_i \cdot s_j$, where s_i, s_j are the spin values in each point of the mesh, with common values of +1 or −1. In our representation, these parameters represent *trans* (+1) or *gauche* (−1) isomerism; and J is the energetic term that considers the magnitude of the interaction between neighbours in the mesh -i.e., coupling-. As this value decreases, the temperature of the transition also decreases. We have applied this model to lipid bilayer systems with embedded surfactants in order to provide a new interpretation of the model parameters proposed by Almeida[32]. Following the analogy, J in the Ising model plays a

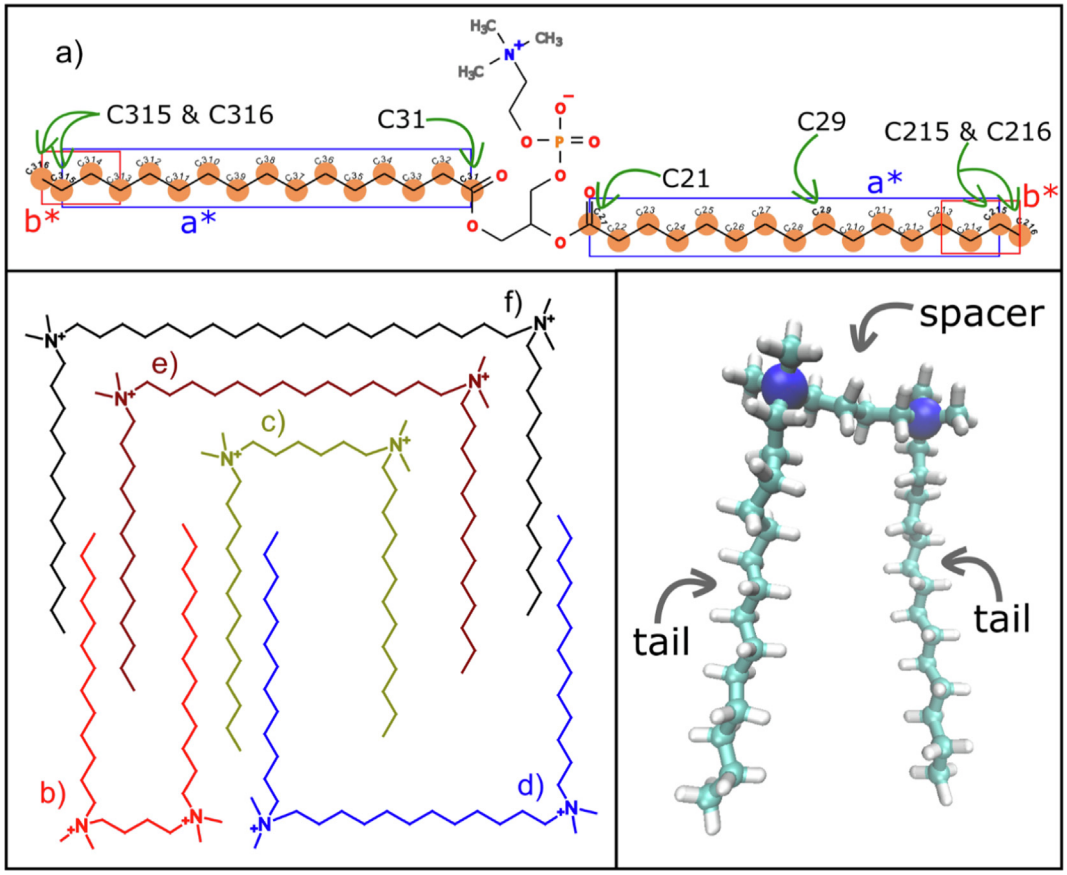

Fig. 1. Molecular structures used along this work. a) DPPC molecule with carbon labelling in the palmitic acid chains. a* and b* show the carbons involved in the dihedrals of the lipid chains, middle and last, respectively. b) Gemini 14-4-14, from now on GS4, and respectively the other surfactants. c) GS6. d) GS12. e) GS14 whit identification of tail and spacer chains. f) GS20.

role in the coupling degree related to the lipid bilayer transition temperature.

This work presents a physicochemical characterization of cationic liposomes, obtained when DPPC is doped with gemini surfactants based on tetradecyltrimethylammonium bromide with varying alkane spacer groups attached to their ammonium headgroups (see Fig. 1). We use DSC data combined with molecular dynamics simulation to unravel the changes induced by the gemini surfactants in the structure and morphology of the lipid bilayer and we interpreted the experimental data with an adapted Ising model. From molecular dynamics simulations we will have an important tool to obtain information about the structure and dynamics of lipid membranes[33] alone or with gemini surfactants. In addition, the colloidal stability of the obtained liposomes is evaluated by DLS, and discussed as regarding the nature and concentration of the partitioned gemini surfactants.

2. Materials and methods

2.1. Materials

The zwitterionic lipid 1,2-dipalmitoyl-*sn-glycero*-3-phosphocholine (DPPC) was purchased from Avanti Polar Lipids, Inc. (USA). The family of gemini surfactants used has two bromides as the anionic counterion, being the differential element the length of the hydrocarbon chain acting as spacer group: N^1,N^1,N^4,N^4-tetramethyl-N^1,N^4-ditetradecylbutane-1,4-diaminium (GS4), N^1,N^1,N^6,N^6-tetramethyl-N^1,N^6-ditetradecylhexane-1,6-diaminium (GS6), N^1,N^1,N^{12},N^{12}-tetramethyl-N^1,N^{12}-ditetradecyldodecane-1,12-diaminium (GS12), N^1,N^1,N^{14},N^{14}-tetramethyl-N^1,N^{14}-ditetradecyltetradecane-1,14-diaminium (GS14), and N^1,N^1,N^{20},N^{20}-tetramethyl-N^1,N^{20}-ditetradecylicosane-1,20-diaminium (GS20). Deionized water was used to prepare all solutions.

The gemini surfactants 1,4-Bis(tetradecyl trimethyl ammonium) butane (GS4), 1,6-Bis(tetradecyl trimethyl ammonium) hexane (GS6) and 1,12-Bis(tetradecyl trimethyl ammonium) dodecane (GS12) were synthesized from the corresponding α,α-dibromide, 1,4-dibromobutane, 1,6-dibromohexane or 1,12-dibromododecane (5 mmol) with anhydrous N,*N*-dimethyltetradecylamine (10 mmol) in 50 mL of acetone under boiling and reflux for 96 h. The material obtained after removal of the solvent with a rotary evaporator was crystallized from ethanol-ether. The obtained crystals (recrystallized from methanol) were then dried in a vacuum desiccator at ambient temperature to give the desired product (25 % yield).

Geminis with larger spacers, GS14 and GS20, were prepared through a similar methodology by using non-commercial dibromides. 1,14-dibromotetradecane and 1,20-dibromoeicosane were obtained from α-bromocarboxylic acids (8-bromooctanoic and 11-bromooctanoic acids, commercially available) by Kolbés electrolysis of the α-bromo carboxylic acids in methanol[34].

The gemini surfactants were characterized by ^{1}H NMR spectroscopy (see Fig. SI1). NMR spectra were measured in a Bruker Advance ARX-400 spectrometer operating at 750 and 300 MHz. The observed ^{1}H NMR shifts (300 MHz, D_2O, 25 °C) for GS4 (Fig. SI1a) were: δ = 3.50 (m, 8H), δ = 3.22 (s, 12H), δ = 1.95 (m, 4H), δ = 1.82 (m, 4H), δ = 1.34 (m, 44H), δ = 0.92 (m, 6H), for GS6 (Fig. SI1b): δ = 3.41 (m, 8H), δ = 3.19 (s, 12H), δ = 1.82 (m, 8H), δ = 1.34 (m, 48H), δ = 0.93 (m, 6H), for GS14 (Fig. SI1c): δ = 3.33 (m, 8H), δ = 3.17 (s, 12H), δ = 1.73 (m, 8H), δ = 1.37 (m, 64H), δ = 0.92 (m, 6H), for GS20 (Fig. SI1d): δ = 3.31 (m, 8H), δ = 3.15 (s, 12H), δ = 1.73 (m, 8H), δ = 1.36 (m, 76H), δ = 0.91 (m, 6H). The ^{1}H NMR shifts (750 MHz, DMSO d_6, 25 °C) for GS12 (Fig. SI1e) were: δ = 3.26 (m, 8H), δ = 3.01 (s, 12H), δ = 1.63 (m, 8H), δ = 1.26 (m, 60H), δ = 0.85 (t, 6H).

2.2. Preparation of gemini-doped liposomes

Following previously described 'film method' [35], appropriate amounts of the DPPC lipid and gemini surfactants were dissolved in 10 mL chloroform, and thereafter a vacuum rotary evaporation method has been used to remove the organic phase. A thin film is obtained, where lipids and gemini surfactants are mixed and spread over the surface of a glass round-flask. The bath temperature of the rotary evaporator was set to 60 °C –above the lipid gel to liquid–crystal transition (∼42 °C) of DPPC lipids. After drying, we hydrated the thin film with pure water for 10 min in an ultrasonic bath at 60 °C to ensure bilayer formation. The final lipid concentration was set at 1.40 mM, suitable for DSC experiments. To reduce the polydispersity of the liposomes, the liposomal dispersion was passed through polycarbonate membranes (Nucleopore, Pleasanton, CA, USA) of 0.1 μm pore size under a 10 bar pressure of N_2 atmosphere, in a 10 mL stainless steel extruder (Lipex Biomembranes, Vancouver, BC, Canada) at 60 °C. Five successive extrusion cycles were carried out. DLS confirm the formation of large unilamellar vesicles (LUVs) with low polydispersity The samples with incorporated gemini surfactant are identified by the DPPC/gemini molar ratio as 1000/1, 100/1, 50/1 and 30/1, respectively.

2.3. Differential scanning calorimetry (DSC)

A SETARAM Micro DSC-III heat flux microcalorimeter with Hastelloy batch vessels (900 μL) was used to determine the thermal behavior of lipid bilayers of systems formed by DPPC liposomes doped with gemini surfactants. Temperature scans between 20 and 50 °C at 0.1 °C/min heating/cooling rate were performed. The measurements were carried out during two heating/-cooling cycles. The reproducibility of thermograms was probed, and the hysteresis between heating/cooling were observed (less than 0.5 °C). The reference cell was filled with deionized water whereas the sample cell contained the liposome suspension. Enthalpograms were analyzed using Calisto SETARAM Software, subtracting a blank (water/water) and a baseline, prior to peak integration to obtain the phase transition temperature T_m, enthalpy change ($\triangle H$), and the peak width.

2.4. Dynamic light scattering (DLS)

A Zetasizer Nano ZS (Malvern Instruments ltd., UK) was used to determine the size, ζ-potential and polydispersity index (PDI) of the liposomes, using the translational diffusion coefficient derived from the autocorrelation function. The NP size and PDI were estimated by applying the Stokes-Einstein equation $d_H = \frac{k_B T}{3\pi\eta D}$ (where k_B is Boltzmann constant, T temperature, η viscosity, D diffusion coefficient and d_H hydrodynamic diameter) and cumulants analysis of the correlation function, while the ζ-potential was estimated through the measuring the electrophoretic mobility by applying Smoluchowskís model $U_E = \frac{2\epsilon\zeta f(\kappa a)}{3\eta}$ (where ϵ is dielectric constant, ζ zeta potential, $f(\kappa a)$ the Henrýs function with value around 1.5 under Smoluchowski approximation and η the viscosity). The calculations and data correlation treatments were carried out with the software provided and tested of Zetasizer Nano SZ from Malvern Instruments, version 8.01.

2.5. Molecular dynamics (MD) simulations

We used computational routines to carry out the analysis of the interaction between gemini surfactants and a lipid bilayer of DPPC molecules. The topology of the gemini residues were obtained and validated with CGenFF, the CHARMM General Force Field server

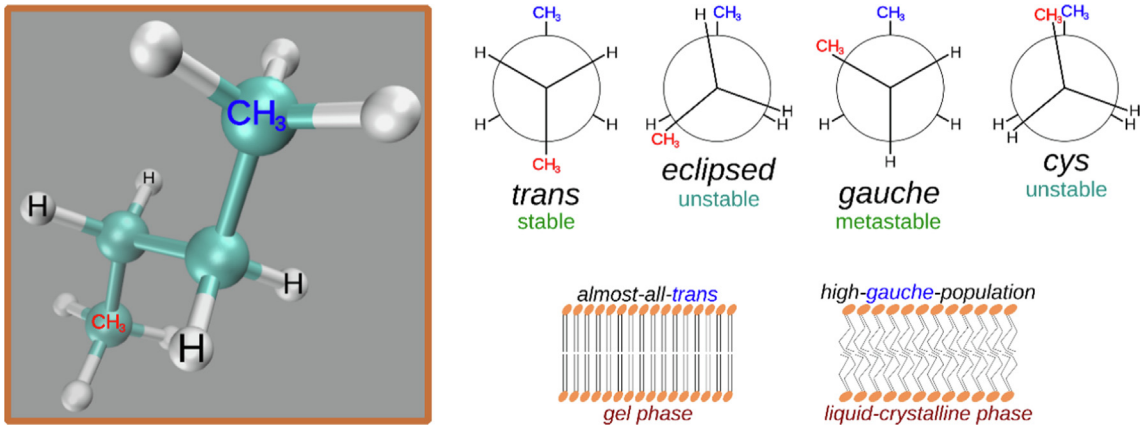

Fig. 2. Representation of butane isomerizations and the relation to *gel* and *liquid–crystal* phases in the lipid bilayer.

[36–39]. A solvated bilayer of 132 DPPC lipids was assembled with CHARMM-GUI Membrane Builder[40–46]. TIP3P[47] water molecules were used, which satisfies a reasonable DPPC/water molecules ratio of approximately 1/45[48]. We use GROMACS[49] functions to insert the geminis in the inner part of the lipid bilayer; likewise, the final system was neutralized by adding two chloride ions in the aqueous medium. We carried out GROMACS runs at two different temperatures, 20 and 50 °C. Each run was previously minimized for 5000 steps in a step-descent algorithm routine. A pair list with buffering was generated by Verlet cutoff-scheme [50], with a cut-off distance for short-range of 1.2 nm. We set Van der Waals type interaction with a cut-off of 1.2 nm, with a van der Waals-modifier of force-switch between 1.0 nm and previous cut-off. Coulomb interactions were implemented by Particle-Mesh Ewald method (PME)[51], with a cut-off set at 1.2 nm. The bonds with H-atoms were converted to constraints by the LINCS algorithm[52]. The canonical (NVT) and isothermal-isobaric (NPT) ensemble equilibrations were carried out for 20 ns. We have selected Berendsen-thermostat[53] to set the temperature coupling, with a reference temperature for coupling of 1 K. The Berendsen exponential relaxation pressure coupling was selected using semi-isotropic conditions due to the symmetry of our nanosystems, in which the Z-axis is normal to the lipid bilayer. The simulations were run for 170 ns; while the temperature coupling was implemented by the Nose-Hoover extended ensemble [54,55]. Likewise, the pressure coupling was set by Parrinello-Rahman extended ensemble[56]. We use VMD software for visualization; in addition, GROMACS functions and Python scripts were used to analyze the trajectories.

3. Results and discussion

3.1. Thermodynamic characterization of gemini-doped DPPC liposomes

Lipid bilayers are examples of a lyotropic phase consisting of bilayers where the lipids have their polar heads exposed to water and the hydrocarbon chains are in the interior of the bilayer. Lipid chains have different conformations because of different dihedral between three consecutive CH_2 groups (*trans* or *gauche* -stable and metastable, respectively-, and *eclipsed* or *cys* -both unstable) (see Fig. 2). A possible characterization method considers two distinct phases, namely gel state and liquid-crystalline, which have different conformational states in the lipid bilayer - almost all *trans* in the gel phase and with a relevant *gauche* population in the liquid-crystalline phase[57–59]. Due to quantum characteristics behind isomerism, *trans*-to-*gauche* exchanges depend only on the available energy to reach the required gap. The conformational energy between *trans*-to-*gauche* isomers in single carbon bonds has an internal barrier energy of 3.8 kJ/mol[60]. This energy gap corresponds to infrared wavelengths and Brownian motion energies. The main molecular compound of the liposomal nanosystem is water, which can be considered the thermal contact with the lipid bilayer. Hence, water molecules at some temperature will transmit energy to the hydrocarbon chain. The bilayer's polar moiety forms a diffusion barrier to the transport of energy between water molecules and the lipid bilayer inner part. The hydrocarbon tails length determines the transition temperature. The energy to explore the different isomers in the dihedrals of carbon chains is similar; the different lengths -different number of dihedrals- imply different energies to reach the transition, denoted by increasing the transition temperature of saturated fatty acid phosphatidylcholine lipids (i.e., DLPC, DMPC, DPPC, DSPC)[61].

Differential scanning calorimetry (DSC) measurements have been performed to determine the transition temperature experimentally[62] of DPPC lipid bilayers doped with different gemini surfactants.

Furthermore, we used the above argument together with the Ising Model to explain the changes in transition temperature of the liposomes induced by the presence of the different gemini surfactants. Fig. 3 and Figures SI2 to SI5 show the DSC enthalpograms of DPPC liposomes doped with GS14, GS4, GS6, GS12 and GS20 gemini, respectively. It can be observed that the transition temper-

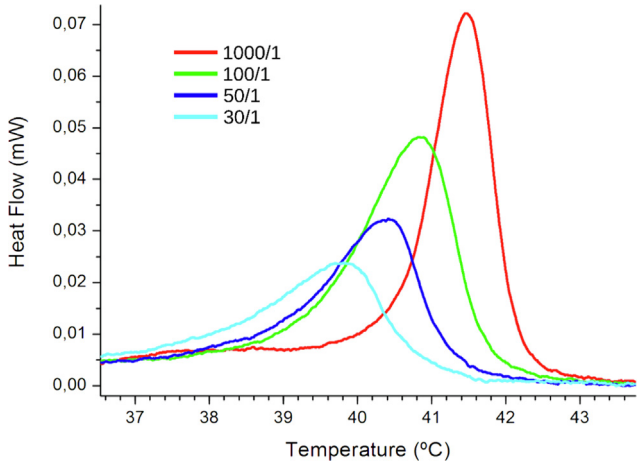

Fig. 3. DSC enthalpograms of DPPC liposomes doped with different amounts of the GS14 surfactant. Each color corresponds to a specific DPPC/GS14 molar ratio.

ature decreases, and the width of the transition peak increases when DPPC liposomes are doped with the gemini surfactants. Fig. 4a shows the transition temperatures, from *gel* to *liquid-crystalline* phase in lipid bilayers, as the gemini surfactant concentration and the spacer group length increase. As observed, the progressive increase in the gemini/lipid ratio leads to a decrease in the liposome transition temperature. The surfactant insertion into the bilayer decreases the hydrophobic interactions between the lipid tails disorganizing them, thus, facilitating the lipid transition to a more fluid phase. Indeed, this decrease is larger as the surfactant

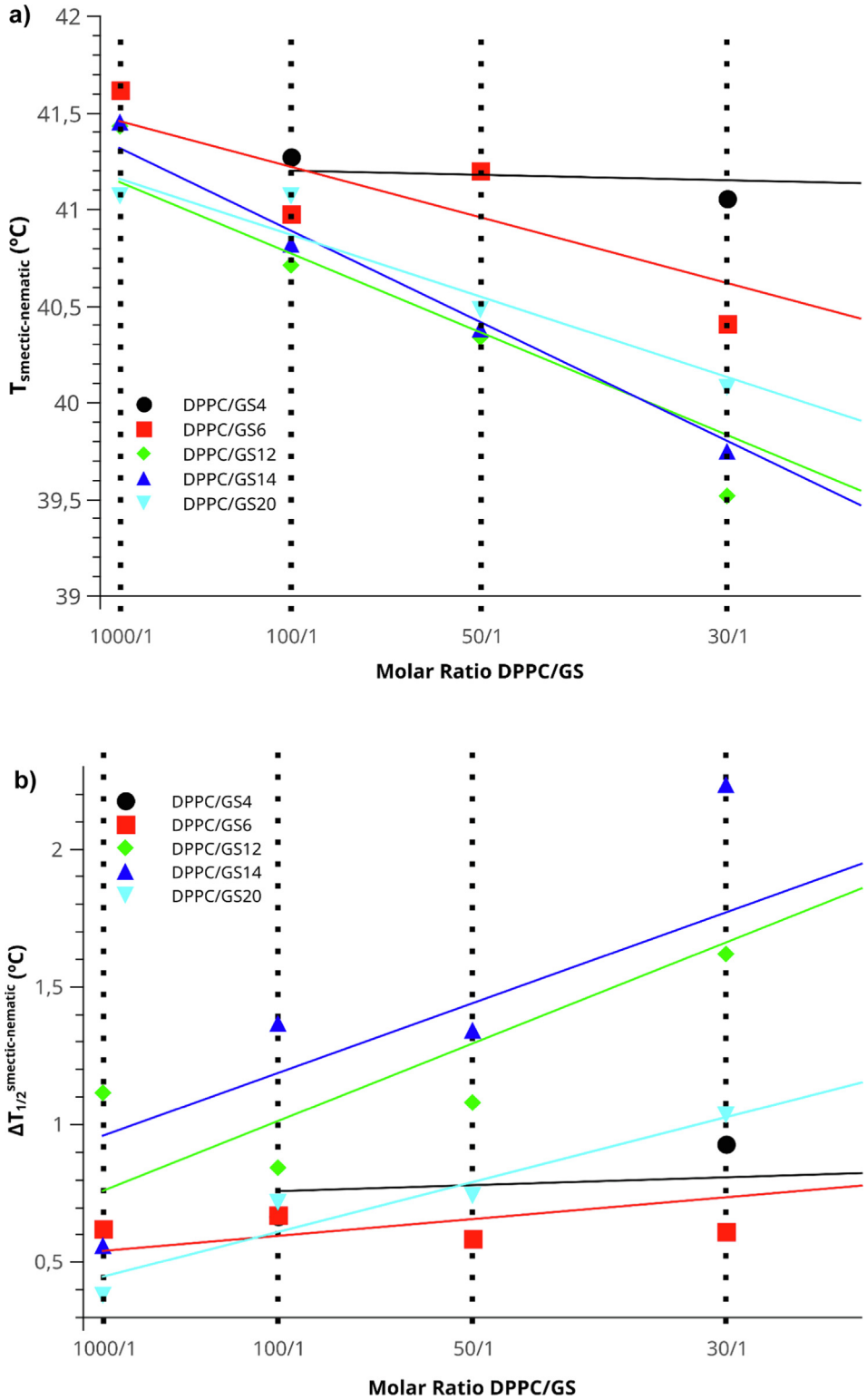

Fig. 4. a) Plot of the transition temperature of the gel-liquid crystalline transition of DPPC *vs* the percentage of gemini surfactant (mol/mol), for various GS spacer lengths. Critical temperatures showed undergoes variations less than 0.3%, taking account the reproducibility in heating/cooling cycles. b) Plot of the change in temperature width at half-height *vs* gemini surfactant concentration (mol/mol), for various GS spacer lengths. Width at half-height temperatures showed undergoes variations less than 10%, taking account the reproducibility in heating/cooling cycles. The lines are just to guide the eye.

concentration increases. This ability of the gemini surfactants might be explained using the transcendent physical paradigm of the Ising model. The presence of gemini surfactants in lipid bilayers would reduce the energetic cost to excite isomerizations in hydrocarbon chains. Hence, one can conclude that the presence of the geminis makes the isomerizations more accessible at lower temperatures, and this trend is enhanced as the gemini concentration rises. We can conclude that, since there are no chemical reactions between the geminis and lipids that could promote molecular orbitals changes, there are no modifications in the energy gaps between isomers. Due to the role of water molecules to supply energy for isomerizations in the hydrocarbon chains, it seems feasible that the presence of the gemini increases the probability of energy transmission from water to the hydrocarbon chains. The decrease of J in the Ising model can be understood as an enhancement of the probability of contacts between CH_2 groups and water molecules moving.

Fig. 4b shows the variation of the temperature width at half height ($\triangle T_{1/2}$) upon changing the gemini surfactant percentage in the system. A more pronounced widening for the transition peaks in the lipid bilayer bearing gemini with spacer groups of 12, 14 or 20 are observed. Conversely, these changes are smoother for spacers with 4 and 6 atoms. Although the presence of gemini surfactants implies a net change in the transition thus decreasing the critical temperature, it is assumed that the probability of CH_2 dihedrals to absorb the isomerization energy is associated with a larger temperature interval when the lipid bilayer has gemini surfactant. When compared to a pure homogeneous DPPC lipid bilayer, blended DPPC/gemini systems have an intrinsic heterogeneity at molecular level. As the critical temperature has been related to the isomerization energy transmission probability, in a heterogeneous system the energy transmission will occur in a larger temperature range than for a homogeneous one. The widening of the transition peak by molecular species partionized into the lipid bilayer has been extensively reported [5,33,63]. In terms of the developed Ising model, this is related to the probability that energy transmission excites isomeric states in CH_2 dihedrals. Gemini surfactants would cause an inhomogeneous distribution of this probability throughout the lipid bilayer. The coupling energy (J) does not have a homogeneous distribution, so the transition temperature is not unique but emerging a temperature transition range.

Fig. 5 shows the enthalpies values upon changes in gemini surfactant concentration. The enthalpy change ($\triangle H$) values are calculated by integration of the heat flow *vs* temperature plots, and normalized to the DPPC content. Transition enthalpies keep constant for molar ratios between 100/1 to 30/1 (DPPC/GS). The previously noted widening of the transition peaks is a handicap to determine such area, basically due to the difficulty to choose a proper baseline. Nevertheless, considering mean values of the set of enthalpies for each gemini/DPPC nanosystem (e.g., GS4/DPPC for all ratios), and being the enthalpy value estimated by dividing the peak area by the DPPC amount, the enthalpy change decreases for all gemini/DPPC systems (inset Fig. 5). Following the role of J as coupling degree, the net decrease in $\triangle H$ is due to a decrease in the interactions between DPPC molecules due to surfactant insertion in the lipid bilayer. Also, the molecular structure differences between gemini surfactants and DPPC lipids favors alterations in the packing of the lamellar membrane. This fact points to the relevance of the way in which the geminis is embeded in the lipid bilayer. While the increase of embedded gemini shows alterations in the lipid bilayer conformation, Fig. 6 shows a remarkable difference in the transition temperature for systems at a 100/1 M ratio for the different spacer lengths. The transition temperature decreases for GS4 and GS6, but increases from GS12 to GS20. Hence, this behaviour at this particular molar ratio could be due to different configurations of the gemini in the lipid bilayer as

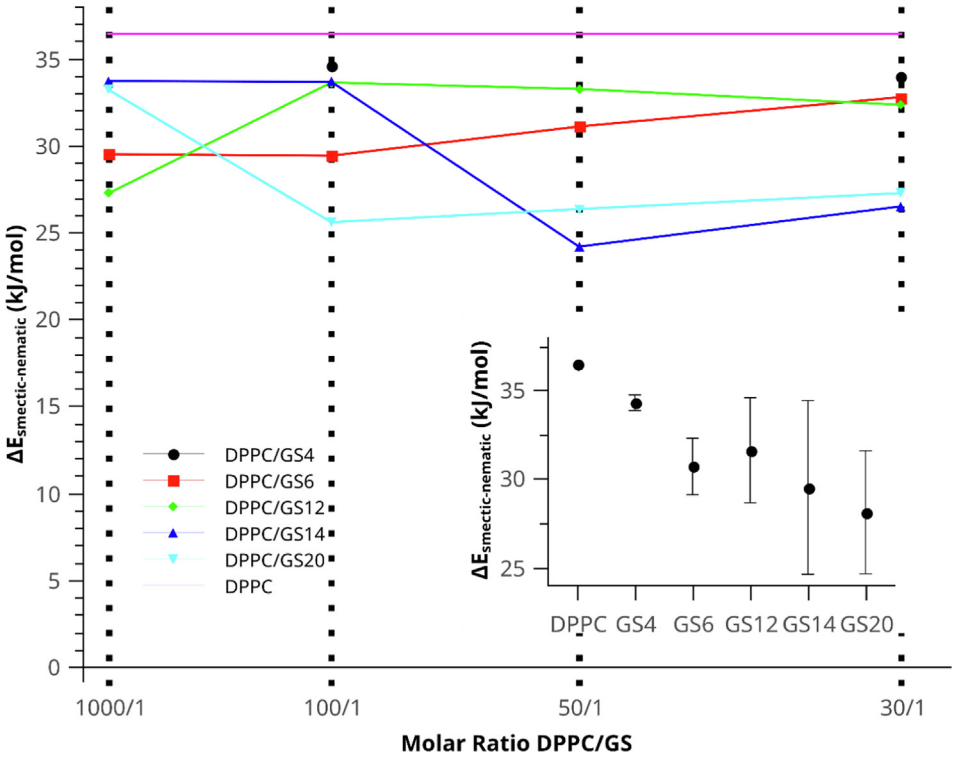

Fig. 5. Variation of the transition enthalpy ($\triangle H$) for DPPC/gemini liposomes *vs* the gemini surfactant content (mol/mol) for various GS spacer lengths. The inset shows the mean values and standard deviations of the enthalpy value for all concentrations per spacer length.

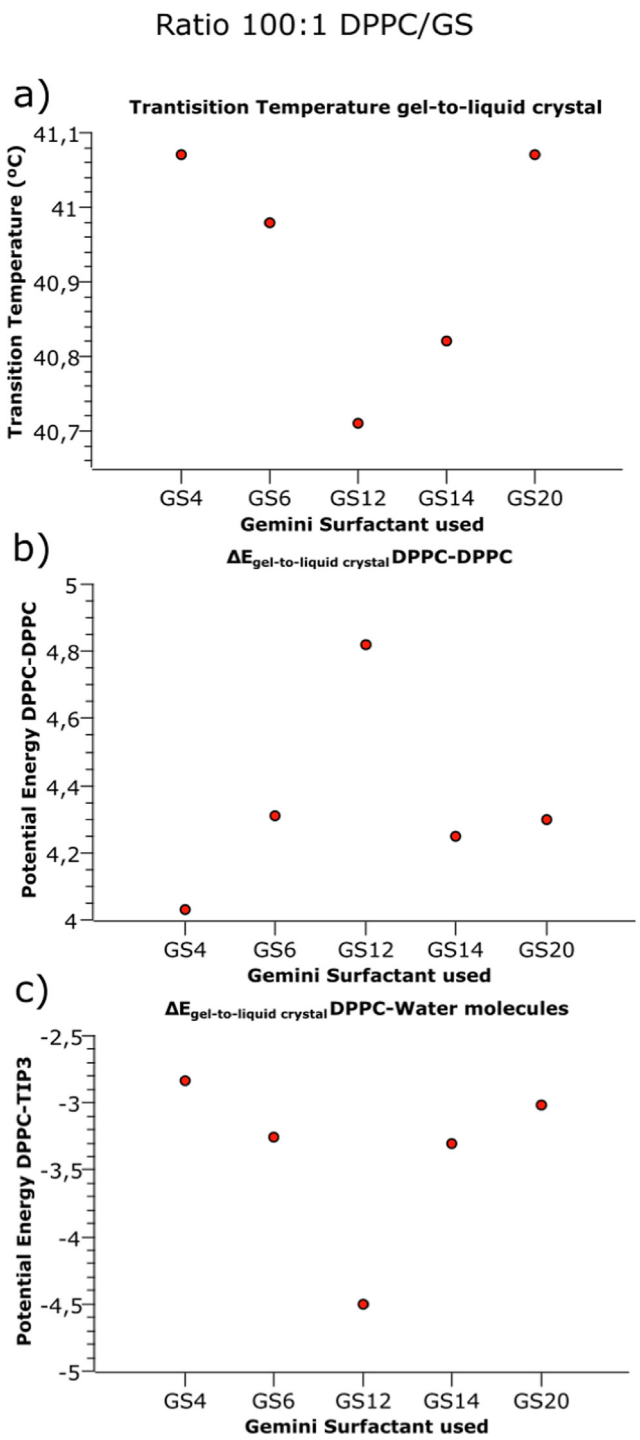

Fig. 6. a) Plot of the changes in transition temperature ($\triangle T_m$) as a function of the gemini spacer length at a 100/1 ratio, as obtained from DSC. Variation of the b) Coulomb interaction energy of DPPC-DPPC and c) DPPC-Water molecules determined by MD for different gemini spacer lengths.

the spacer length increases. To confirm such hypothesis, we perform molecular dynamics simulations of the DPPC lipid bilayer and the gemini surfactants.

3.2. MD simulations of DPPC bilayers with incorporated gemini surfactants

We use molecular dynamics simulations to predict the positioning and interaction of the gemini surfactants within the lipid bilayer. We carried out five simulations, one per each surfactant spacer length, at two different temperatures 20 and 50 °C. These temperatures were selected because they are below and above the lipid transition temperature measured by DSC. Fig. 7 shows snapshots for each simulation in a final instant corresponding to equilibrium, in energetic terms. At 20 °C, GS4 and GS6 have a preferred location by orienting their two polar heads with the outermost part of the lipid bilayer, whereas GS12, GS14 and GS20 show a unique accommodation (Video SI1). Each of their polar heads is oriented to one of the opposing layers of the lipid bilayer. Immediately, the implications of this different positioning in transmembrane potential are evident. Fig. 8 shows that the electrostatic profiles manifest local asymmetry differences whether the spacer is long or short. In particular, the difference of transmembrane potential for GS4 and GS6 is considerably more significant than for GS12, GS14 or GS20. The density profiles of N + of each of the two quaternary ammonium heads show changes in their positions with the spacer group length. GS4 and GS6 arrange their two electrical charges on one side of the lipidic membrane (either internal or externally), while GS12, GS14 and GS20 locate them at both sides, that is, one charge on the outer face and the other on the inner face of the bilayer. This symmetric and asymmetric localization is responsible of the local electrostatic potential differences along the blended lipid membrane. Simultaneously, Fig. 8 also shows the gemini density profiles and N atoms of the DPPC. GS4 and GS6 show again their distribution at only one side, whilst GS12, GS14 and GS20 show a deeper embedment within the bilayer.

Due to the significant differences in the positioning of the different geminis, the molecular dynamics trajectories help in assessing the role of the gemini on the conformation behaviour of lipids in the bilayer. Fig. 9 shows the radial distribution functions (RDF), centering the reference in C29 (see Fig. 1). At 20 °C the RDF for all nanosystems shows six peaks, corresponding with the sixth neighbours' correlation. This coupling suggests a gel conformational phase in the lipid bilayer. At 50 °C, the RDF shows only three peaks, reflecting a decrease in the correlation order until a third neighbourś coupling, which agrees with a liquid crystal conformational state. The RDFs were computed separately for each membrane layer, confirming the absence of a significant interaction of the gemini surfactants into the bilayer's conformational state.

Nevertheless, in the snapshots of Fig. 7 a significative difference at 20 °C appears: whilst for a pure DPPC bilayer the lipid alkyl chains form a cross-tilted conformation[64–67] between both layers, when a gemini is embedded that alignment becomes partially cross-tilted (GS4 and GS6) or completely tilted (GS12, GS14 and GS20). We did not observe such an effect in the RDF of Fig. 9 because the coordination between lipids is the same for both tilted organizations. On the other hand, Fig. SI9 shows the angle between C216-C21 and C316-C31 vectors at top and bottom layers by averaging all lipids during the last 50 ns of the simulations. As seen, the average orientation for pure DPPC bilayers shows the cross-tilted direction between layers; in contrast, when the gemini is incorporated, the angle between top and down vectors is closer to 180°, reflecting a tilted organization. The differences about these gel conformations may play a crucial role in membrane permeability [68]. In this way, the presence of gemini surfactants involves changes in the lipid membrane, vanishing the cross-tilted organization and favouring the tilting in one direction. Fig. SI10 shows tilt angles of the lipid chains with respect to the Y and Z-axes. The embeddement of the gemini modifies the cross-tilting due to the molecular structure differences between pure and surfactant-doped DPPC bilayers. Visually in Fig. 7, the location of GS4 and GS6 consists of a parallel positioning of the surfactant tails respect to the lipid alkyl chains. The electrostatic interaction between the N^+ atom of the gemini surfactant and the bilayer's polar region does not allow

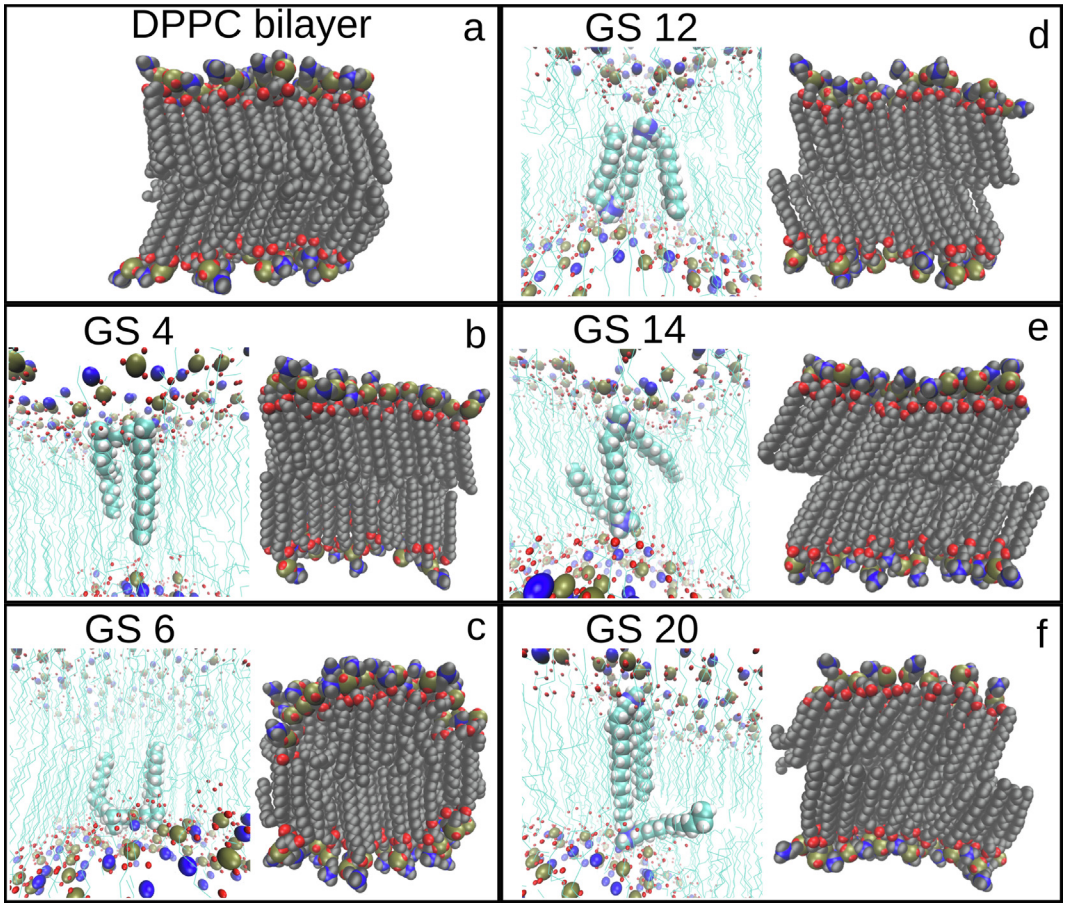

Fig. 7. Snapshots of the simulations at 20 °C for each doped-liposome nanosystem. Right images show the lipid bilayer conformation and left ones the inner part of the lipid bilayer highlighting the location of gemini surfactant. a) Pure DPPC. b) DPPC:GS4. c) DPPC:GS6. d) DPPC:GS12. e) DPPC:GS14. f) DPPC:GS20.

a parallel orientation of the spacer group toward lipid chains. However, when the spacer group is long enough, both tails and spacer of GS12, GS14 and GS20 accommodate parallelly to the lipid chains. The only possibility of satisfying this "staple" role is by inducing one-directional tilting between two monolayers.

As discussed in previous sections, differences between *gel* or *liquid–crystal* conformational phases are based on the dihedral between consecutive C—C bonds. Fig. SI11 shows the criterium to identify the conformation between such bonds. We computed the dihedrals between consecutive C—C bonds for all DPPC molecules during the last 50 ns of each simulation. Table 1 shows all mean values of dihedrals between bonds in lipid chains. We observe a significant difference between the percentage of *gauche* population between C315-C31 or C215-C21 and C316-C313 and C216-C213. The difference between *trans-eclipse-gauche* percentage populations at different temperatures together with polar head interactions, is related to the phase transition in the lipid bilayers [69]. We can observe very slight differences between the percentage of *gauche* population at 20 °C between pure and gemini-doped DPPC bilayer systems (see *a* and *b* values in Table 1). The DPPC pure bilayer shows the highest *gauche* ratio value at 20 °C; this fact will point again to the gemini surfactant's ability to absorb the needed energy to change its conformation before DPPC so that the gemini surfactant will favour the *trans* configuration of the lipid chains. Table 2 shows the mean percentage values at 20 °C and 50 °C for the tails and spacers of the gemini surfactants, manifesting that these differences are not significant as occurred for the lipids. To show the nature of the energy flow detected in DSC measurements, we used the MD trajectories to calculate an approximate value of the energy changes between 20 °C and 50 °C (*get*-to-*liquid–crystal*). We should consider that the palmitic chains of DPPC allow 26 dihedrals (see Fig. 1), 24 of them configure the internal backbone whereas the other two form the end of the chains. Assuming the energy values of the isomerizations of the butane[60]: $\Delta E_{eclipsed}$ = 16,0 kJ/mol and ΔE_{gauche} = 3,8 kJ/mol, which describes only one dihedral; we calculate the energy values (see Table 3) by using the difference in the percentage of *gauche* and *eclipsed* populations between the two temperatures. Moreover, the variations of non-bonded energies were calculated by computing the Coulomb and Lennard-Jones energies for DPPC-DPPC and DPPC-water molecular interactions (see Table 3). We estimate the energy variation between both temperatures by summing the contribution energies of *gauche*, *eclipsed*, DPPC-DPPC and DPPC-water. The obtained values highly agree with enthalpy values obtained from DSC data, confirming that the *trans*-to-*gauche* and the unstable state eclipsed isomerizations play the principal role in the transition energy. Indeed, the relation between Coulomb electrostatic energy between DPPC-DPPC and DPPC-Water molecules in Fig. 6b,c agrees with the variation of transition temperature for nanosystems at a ratio of 100/1 as seen in Fig. 6a. Following the previous relationship between the coupling energy (J) in the Ising model and the transmission energy probability, the molecular dynamics results shown in Fig. 6c well agree, showing a notable correspondence between the transition temperature variation and the interaction energy between DPPC and water molecules.

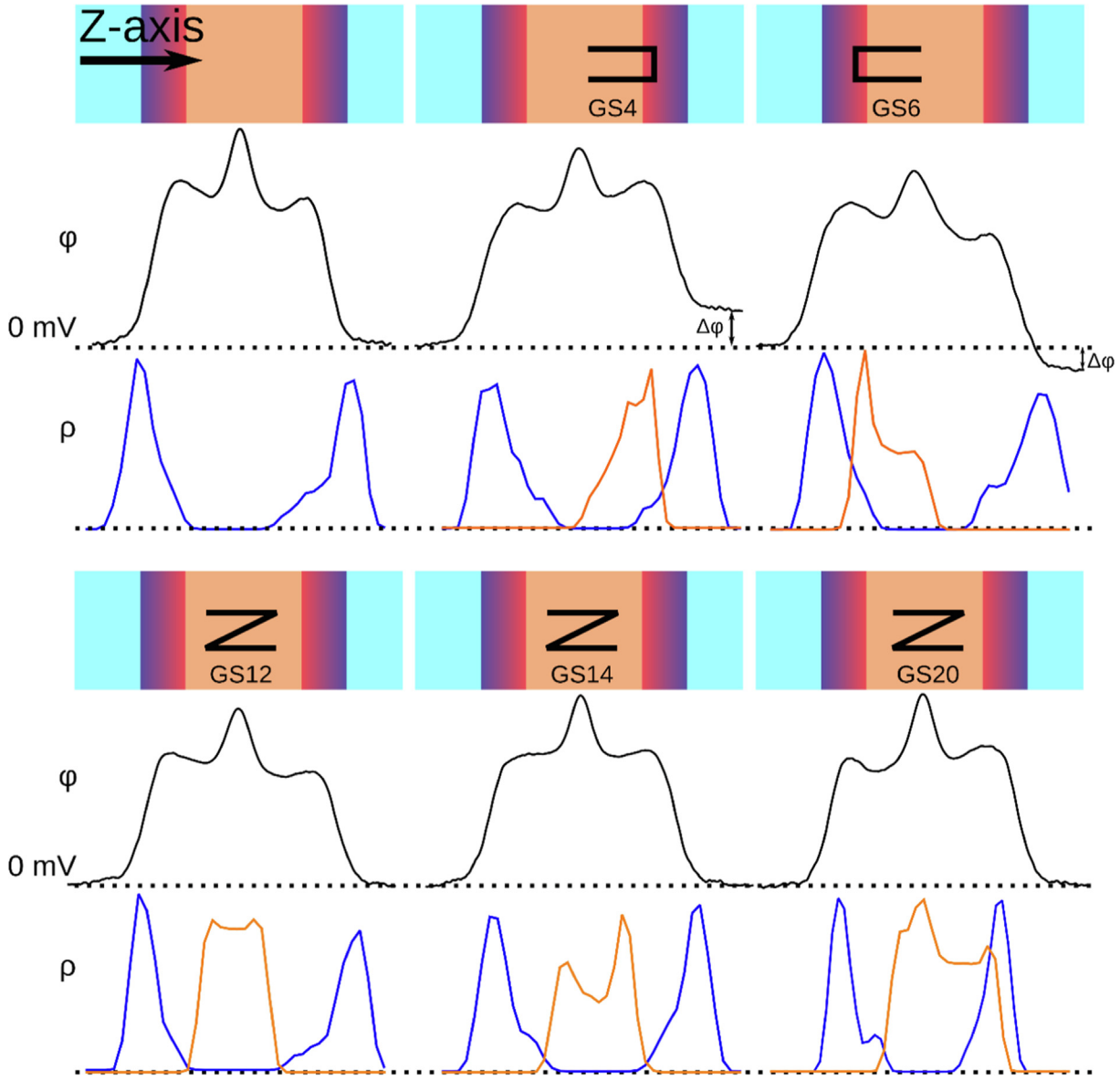

Fig. 8. Plot of the transmembrane potential (black lines) and density profiles of N for DPPC (blue) and gemini surfactants centre of masses (orange). Color representations show a simplistic scheme of the lipid bilayer along Z-axis, and black "staples" represent the gemini surfactant. Both potential and density profiles were computed from the last 50 ns of the molecular dynamic simulations at 20 °C.

So far, it has been shown that differences in the lipid bilayer's inner part are induced by the presence of gemini surfactant and that the spacer length also plays a key role. Concerning the modifications in the DPPC polar moiety, the localization of the N + of the gemini implies that the surface density charge of liposomes is more positive. In fact, the details of the simulation help us to obtain more information about the polar behavior (orientation changes of the head group of the lipid) of DPPC in the bilayer, for example, by observing the angle of the vector of the P-N moiety of the DPPC polar head respect to the normal direction of the bilayer in the Z-axis direction, as shown in Fig. 10. The presence of the gemini induces a decrease of the angle, slightly exposing the N + residue of the lipids to the bulk water. This means that the overall cationic behavior of liposomes is not only due to the pure contribution of N + of geminis, but also to an induced reorientation of the P-N moiety of DPPC headgroups.

3.3. Analysis of the colloidal stability of gemini-doped liposomes

We used dynamic light scattering (DLS) measurements to determine changes in surface density charge of DPPC/gemini liposomes and to evaluate their colloidal stability. Since DSC data and MD results confirmed the ability of the geminis to partition into and modify the lipid bilayer, DLS data will provide information about changes in size and zeta potential of the DPPC liposomes doped with gemini surfactants. Regarding the size, pure DPPC liposomes show a hydrodynamic radius of 400(40) nm with a high polydispersity index (PDI) of 0.5 before extrusion. These values are typical of oligolamellar vesicles. The surface charge of such liposomes is + 3.05(1) mV. After several extrusions through a 100 nm pore size membrane, both hydrodynamic radius and PDI decreases, with values of 51(2) nm and 0.125, respectively, whereas no changes were detected in zeta potential.

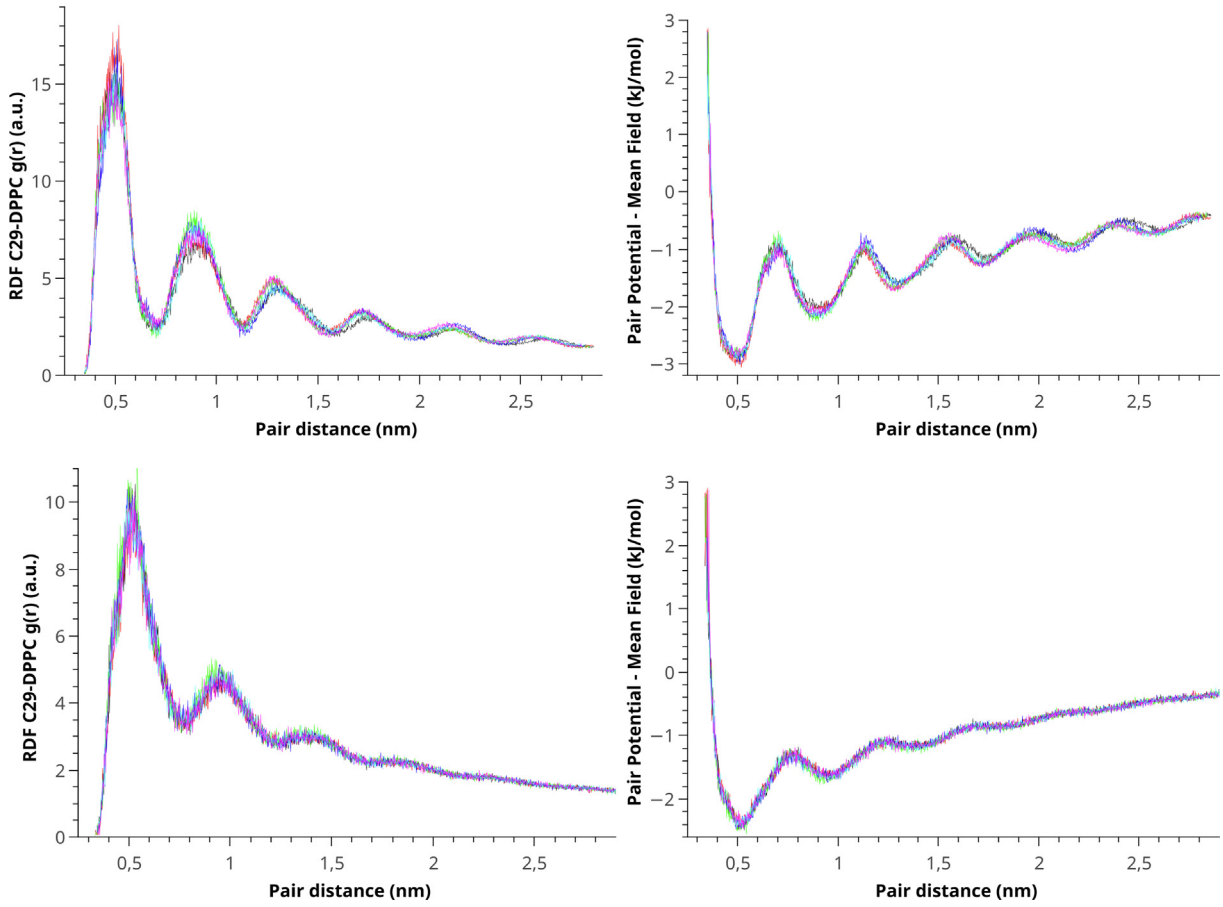

Fig. 9. Plot of the radial distribution functions (RDF) and pair potential of mean-field for the C29 of DPPC (see Fig. 1a). Upper plots correspond to 20 °C, and bottom ones to 50 °C. RDF were computed using the last 50 ns of the molecular dynamic trajectories.

Table 1
Percentages of isomerisms calculated by computing the dihedrals of the palmitic chain of DPPC along the last 50 ns of molecular dynamics trajectories.

Percentages of conformation C—C to C—C at 20 °C – DPPC												
	DPPC		DPPC/GS4		DPPC/GS6		DPPC/GS12		DPPC/GS14		DPPC/GS20	
	a	b	a	b	a	b	a	b	a	b	a	b
trans	90,38	75,82	90,68	76,82	90,43	77,23	91,29	77,06	90,63	76,93	90,93	78,14
eclipsed	2,51	3,74	2,45	3,66	2,55	3,67	2,41	3,64	2,53	3,67	2,45	3,61
gauche	7,09	20,40	6,85	19,48	7,00	19,06	6,30	19,25	6,82	19,36	6,60	18,21
cis	0,02	0,04	0,02	0,05	0,01	0,05	0,01	0,05	0,02	0,04	0,02	0,05
Percentages of conformation C—C to C—C at 50°C – DPPC												
	DPPC		DPPC/GS4		DPPC/GS6		DPPC/GS12		DPPC/GS14		DPPC/GS20	
	a	b	a	b	a	b	a	b	a	b	a	b
trans	69,60	61,30	69,49	61,32	69,60	61,27	69,18	61,20	70,15	61,51	69,64	61,32
eclipsed	6,34	5,81	6,30	5,85	6,33	5,89	6,36	5,81	6,23	5,81	6,31	5,83
gauche	23,97	32,78	24,13	32,72	23,98	32,73	24,37	32,88	23,54	32,56	23,97	32,74
cis	0,08	0,11	0,08	0,11	0,09	0,11	0,09	0,12	0,09	0,12	0,09	0,11

a* the percentages of dihedrals between C215-C21 and C315-C31 (see Fig. 1).
b* the percentages of dihedrals between C216-C213 and C316-C313 (see Fig. 1).

Fig. SI6 shows the intensity profile distribution of the liposomal nanosystems formed by 100/1 ratio mixtures of DPPC and gemini with different spacer lengths. Mean values of R_H and PDI values of 64(13) nm and 0.23 revealed that the inclusion of gemini surfactant in the liposome formation drastically reduces their size and PDI previous the extrusions. The size decrease compared to pure DPPC vesicles can be understood as a decrease of the lamellarity induced by the gemini surfactant. In addition, zeta potential values increase up to ca. + 37(4) mV, indicative of the increase in positive charge consequence of the gemini partition to DPPC membrane. There are no significant differences in the values of positive zeta potential upon changes in the gemini spacer group length. It is relevant here to note that the different gemini positioning observed by MD -U or N form- in the lipid bilayer does not imply differences

Table 2
Percentages of isomerisms calculated computing the dihedrals of the tail and spacer (sp) groups of gemini surfactants along the last 50 ns of molecular dynamics trajectories.

Percentages of conformation C—C to C—C at 20 °C – GEMINI										
	GS4		GS6		GS12		GS14		GS20	
	tail	sp	tail	sp	tail	sp	tail	sp	tail	sp
trans	73,74	96,82	86,91	35,85	78,57	83,48	71,16	82,04	81,46	73,80
eclipsed	2,67	3,18	2,63	1,73	2,65	1,82	3,65	2,64	2,61	3,00
gauche	23,49	0,00	10,44	62,34	18,78	14,70	25,12	15,32	15,90	23,18
cis	0,10	0,00	0,02	0,09	0,00	0,00	0,07	0,00	0,03	0,01
Percentages of conformation C—C to C—C at 50 °C – GEMINI										
	GS4		GS6		GS12		GS14		GS20	
	tail	sp	tail	sp	tail	sp	tail	sp	tail	sp
trans	73,74	90,73	73,55	44,32	68,29	60,45	65,47	81,44	66,86	72,41
eclipsed	4,70	5,34	5,00	2,14	5,20	3,07	4,89	3,43	4,96	4,52
gauche	21,51	3,92	21,42	53,49	26,43	36,37	29,59	15,10	28,13	23,02
cis	0,05	0,00	0,03	0,04	0,08	0,11	0,05	0,03	0,05	0,05

Table 3
Energy variation between 20 and 50 °C taking account the gauche and eclipse isomerizations and the non-bonded interactions (van der Waals and Coulomb) between DPPC-DPPC and DPPC-water molecules (TIP3).

kJ/mol_{DPPC}	DPPC	DPPC/GS4	DPPC/GS6	DPPC/GS12	DPPC/GS14	DPPC/GS20
ΔE_{gauche}	15,37	15,48	15,23	15,86	15,89	15,53
$\Delta E_{eclipse}$	16,34	16,77	16,52	17,52	16,25	16,95
$\Delta E_{DPPC\text{-}DPPC}$	3,84	4,03	4,31	4,82	4,25	4,30
$\Delta E_{DPPC\text{-}TIP3}$	−2,49	−2,84	−3,26	−4,50	−3,30	−3,02
ΔE_{Total}	33,06	33,44	32,80	33,69	32,10	33,75

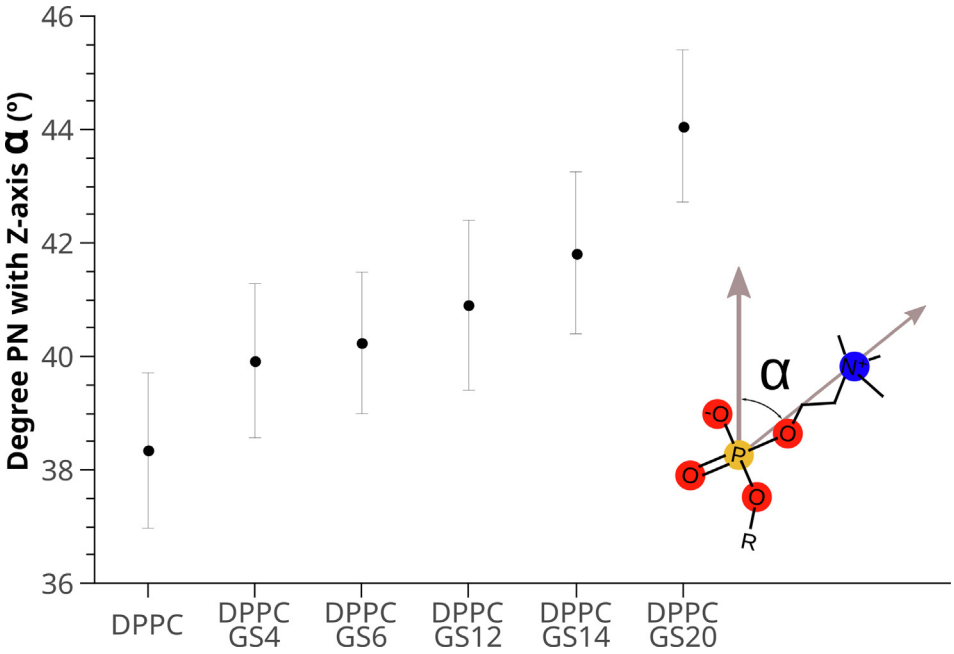

Fig. 10. Average P-N vector angles to Z-axis computed during the last 50 ns of the dynamic simulation trajectory. α is the degree between the P-N vector with the normal direction of the bilayer in the Z-axis direction. The angles represented were computed from simulations at 20 °C.

in the surface density of N + as the ratio DPPC/gemini is kept contant. Fig. SI7 shows a subtle increase between GS4 and GS20, though the main difference in zeta potential values take place between pure and blended liposomes. The increase in positive zeta potential values start to be shown even at a ratio as low as 1000/1. Finally, the extrusion of the as-obtained gemini-doped liposomes additionally decreases the size and PDI values to 47(1) nm and 0,12(5), respectively, as observed in Fig. SI8.

We also tested the colloidal dispersion stability of the cationic gemini-doped liposomes for three months upon storage at 4 °C by DLS. No significant changes in liposome sizes were observed, thus, confirming the colloidal stability of liposomes when incorporating the geminis in contrast to the variation observed for pure DPPC liposomes, for which a progressive size increment was observed (Fig. 11).

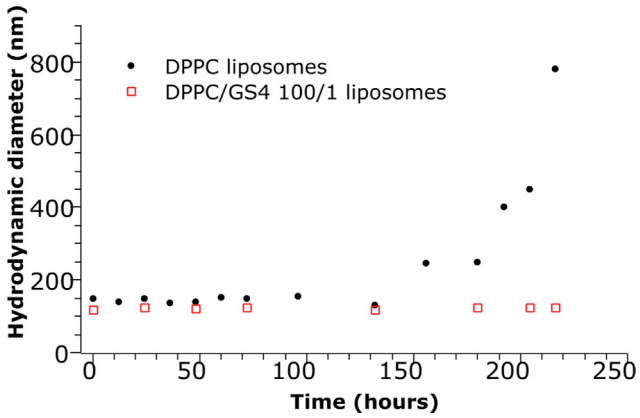

Fig. 11. Variation of DPPC liposomes and DPPC/GS4 doped liposomes during at a ratio of 100/1 for 225 h.

In summary, these results allow us to conclude that the embedment of the gemini surfactants in the lipid bilayer induce small sized liposomes even before that extrusion process, and provides them with a cationic character with long colloidal stabilities.

4. Conclusions

The ability of these gemini surfactants to partition to DPPC lipid bilayer has assessed. DSC measurements show that the transition temperature decreases as the gemini content increases, and also that the surfactants with spacer lengths of 12, 14 and 20 reduce more significantly the transition temperature. At the particular 100/1 ratio the transition temperature decreases gradually for GS4 and GS6, but increasing for GS12 to GS20.

The observed phase transition was interpreted in terms of Ising model parameters and explained by molecular dynamics simulations. The increase in width at half heigh points to an inhomogeneous distribution of coupling terms of the Ising model when the gemini surfactants are incorporated into DPPC liposomes. DLS measurements show a decrease in PDI and size of the DPPC/gemini liposomes mixed prior to liposome extrusion. More interestingly, Zeta potential data show the cationic character of liposomes upon addition of the positively charged gemini surfactants. In agreement to these experimental measurements, molecular dynamics simulations show the localization of the gemini inside the lipid bilayer. The localization and position within the lipid bilayer depends on the spacer group length - GS4 and GD6 6 are positioned in a single face of the bilayer, whilst GS12, GS14 and GS20 allocate each one of their polar heads to opposite layers of the membrane. Monitoring the size of the doped liposomes for a long period, the observed constant size shown the increase in colloidal stability of DPPC liposomes doped with cationic gemini surfactants.Overall this shows that these cationic liposomes have the potential to be used to successful gene therapies, vaccines or biosensor technologies.

CRediT authorship contribution statement

Vicente Domínguez-Arca: Conceptualization, Methodology, Validation, Formal analysis, Investigation, Writing – original draft, Writing – review & editing, Visualization. **Juan Sabín:** Methodology, Investigation, Validation, Writing – original draft, Writing – review & editing. **Luís García-Río:** Methodology, Investigation, Validation, Writing – original draft. **Margarida Bastos:** Validation, Writing – original draft, Writing – review & editing. **Pablo Taboada:** Methodology, Investigation, Writing – original draft, Funding acquisition. **Silvia Barbosa:** Methodology, Investigation, Writing – original draft, Funding acquisition. **Gerardo Prieto:** Supervision, Conceptualization, Writing – original draft, Funding acquisition.

Data availability

Data will be made available on request.

Declaration of Competing Interest

The authors declare that they have no known competing financial interests or personal relationships that could have appeared to influence the work reported in this paper.

Acknowledgments

This work was supported by the Spanish Research Agency (AEI) under Project PID2019-109517RB-I00. ERDF funds are also acknowledged. Facilities provided by the Galician Supercomputing Centre (CESGA) are also acknowledged

Appendix A. Supplementary material

Supplementary data to this article can be found online at https://doi.org/10.1016/j.molliq.2022.120230.

References

[1] M.J. Mitchell, M.M. Billingsley, R.M. Haley, M.E. Wechsler, N.A. Peppas, R. Langer, Engineering precision nanoparticles for drug delivery, Nat. Rev. Drug Discovery 20 (2) (2021) 101–124.
[2] A.D. Bangham, R.W. Horne, Negative staining of phospholipids and their structural modification by surface-active agents as observed in the electron microscope, J. Mol. Biol. 8 (1964) 660-IN10.
[3] J.O. Eloy, M. Claro de Souza, R. Petrilli, J.P.A. Barcellos, R.J. Lee, J.M. Marchetti, Liposomes as carriers of hydrophilic small molecule drugs: Strategies to enhance encapsulation and delivery, Colloids Surf., B 123 (2014) 345–363.
[4] L. Sercombe, T. Veerati, F. Moheimani, S.Y. Wu, A.K. Sood, S. Hua, Advances and Challenges of Liposome Assisted Drug Delivery, Front. Pharmacol. 6 (2015) 286.
[5] V. Domínguez-Arca, R.R. Costa, A.M. Carvalho, P. Taboada, R.L. Reis, G. Prieto, I. Pashkuleva, Liposomes embedded in layer by layer constructs as simplistic extracellular vesicles transfer model, Mater. Sci. Eng., C 121 (2021) 111813.
[6] J. Sabín, J.M. Ruso, A. González-Pérez, G. Prieto, F. Sarmiento, Characterization of phospholipid+semifluorinated alkane vesicle system, Colloids Surf., B 47 (1) (2006) 64–70.
[7] C.N.C. Sobral, M.A. Soto, A.M. Carmona-Ribeiro, Characterization of DODAB/DPPC vesicles, Chem. Phys. Lipids 152 (1) (2008) 38–45.
[8] E.A. Ho, E. Ramsay, M. Ginj, M. Anantha, I. Bregman, J. Sy, J. Woo, M. Osooly-Talesh, D.T. Yapp, M.B. Bally, Characterization of Cationic Liposome Formulations Designed to Exhibit Extended Plasma Residence Times and Tumor Vasculature Targeting Properties, J. Pharm. Sci. 99 (6) (2010) 2839–2853.
[9] V. Rajendran, S. Rohra, M. Raza, G.M. Hasan, S. Dutt, P.C. Ghosh, Stearylamine Liposomal Delivery of Monensin in Combination with Free Artemisinin Eliminates Blood Stages of Plasmodium falciparum in Culture and P. berghei Infection in Murine Malaria, Antimicrob. Agents Chemother. 60 (3) (2016) 1304–1318.
[10] S. Koirala, B. Roy, P. Guha, R. Bhattarai, M. Sapkota, P. Nahak, G. Karmakar, A.K. Mandal, A. Kumar, A.K. Panda, Effect of double tailed cationic surfactants on the physicochemical behavior of hybrid vesicles, RSC Adv. 6 (17) (2016) 13786–13796.
[11] C. Montis, S. Sostegni, S. Milani, P. Baglioni, D. Berti, Biocompatible cationic lipids for the formulation of liposomal DNA vectors, Soft Matter 10 (24) (2014) 4287–4297.
[12] J.A.S. Almeida, E.F. Marques, A.S. Jurado, A.A.C.C. Pais, The effect of cationic gemini surfactants upon lipid membranes. An experimental and molecular dynamics simulation study, Phys. Chem. Chem. Phys. 12 (2010) 14462–14476.
[13] S. Aleandri, C. Bombelli, M.G. Bonicelli, F. Bordi, L. Giansanti, G. Mancini, M. Ierino, S. Sennato, Fusion of gemini based cationic liposomes with cell membrane models: implications for their biological activity, Biochimica et Biophysica Acta (BBA) -, Biomembranes. 1828 (2013) 382–390.
[14] E. Feitosa, F.R. Alves, A. Niemiec, M. Real Oliveira, C.D. Elisabete, E.M.S. Castanheira, A.L.F. Baptista, Cationic Liposomes in Mixed Didodecyldimethylammonium Bromide and Dioctadecyldimethylammonium Bromide Aqueous Dispersions Studied by Differential Scanning Calorimetry, Nile Red Fluorescence, and Turbidity, Langmuir 22 (2006) 3579–3585.

[15] R. Zana, J. Xia, Applications of Gemini Surfactants, CRC Press, 2003.
[16] A.M.S. Cardoso, H. Faneca, J.A.S. Almeida, A.A.C.C. Pais, E.F. Marques, M.C.P. de Lima, A.S. Jurado, Gemini surfactant dimethylene-1,2-bis (tetradecyldimethylammonium bromide)-based gene vectors: A biophysical approach to transfection efficiency, Biochim. Biophys. Acta (BBA) - Biomembr. 1808 (1) (2011) 341–351.
[17] J.A.S. Almeida, H. Faneca, R.A. Carvalho, E.F. Marques, A.A.C.C. Pais, F. Fraternali, Dicationic Alkylammonium Bromide Gemini Surfactants. Membrane Perturbation and Skin Irritation, PLOS ONE 6 (11) (2011) e26965.
[18] B. Brycki, A. Szulc, Gemini Alkyldeoxy-D-Glucitolammonium Salts as Modern Surfactants and Microbiocides: Synthesis, Antimicrobial and Surface Activity, Biodegradation, PLOS One 9 (2014) e84936.
[19] B.E. Brycki, I.H. Kowalczyk, A.M. Szulc, J.A. Brycka, Quaternary Alkylammonium Salts as Cleaning and Disinfectant Agents, Tenside, Surfactants, Deterg. 55 (6) (2018) 432–438.
[20] K. Winnicki, K. Łudzik, A. Żabka, J.T. Polit, A. Zawisza, J. Maszewski, Anti-algal activity of the 12-5-12 gemini surfactant results from its impact on the photosynthetic apparatus, Sci. Rep. 11 (2021) 2360.
[21] M. Pakiet, I. Kowalczyk, R. Leiva Garcia, R. Moorcroft, T. Nichol, T. Smith, R. Akid, B. Brycki, Gemini surfactant as multifunctional corrosion and biocorrosion inhibitors for mild steel, Bioelectrochemistry 128 (2019) 252–262.
[22] B.E. Brycki, Multifunctional Gemini Surfactants: Structure, Synthesis, Properties and Applications, in: Iwona H. Kowalczyk (Ed.), Application and Characterization of Surfactants, IntechOpen, Rijeka, 2017, pp. Ch. 4.
[23] V. Domínguez-Arca, J. Sabín, P. Taboada, L. García-Río, G. Prieto, Micellization thermodynamic behavior of gemini cationic surfactants. Modeling its adsorption at air/water interface, J. Mol. Liquids 308 (2020) 113100.
[24] R. Zana, State of Gemini Surfactants in Solution at Concentrations below the Cmc, CRC Press, 2003.
[25] R. Zana, M. In, Phase Behavior of Gemini Surfactants, CRC Press, 2003.
[26] Y. Han, Y. Wang, Aggregation behavior of gemini surfactants and their interaction with macromolecules in aqueous solution, Phys. Chem. Chem. Phys. 13 (2011) 1939–1956.
[27] I.S. Oliveira, M. Lo, M.J. Araújo, E.F. Marques, Temperature-responsive self-assembled nanostructures from lysine-based surfactants with high chain length asymmetry: from tubules and helical ribbons to micelles and vesicles, Soft Matter 15 (2019) 3700–3711.
[28] V. Walter, C. Ruscher, O. Benzerara, C.M. Marques, F. Thalmann, A machine learning study of the two states model for lipid bilayer phase transitions, Phys. Chem. Chem. Phys. 22 (34) (2020) 19147–19154.
[29] D. Marsh, A. Watts, P.F. Knowles, Cooperativity of the phase transition in single- and multibilayer lipid vesicles, Biochim. Biophys. Acta (BBA) - Biomembr. 465 (3) (1977) 500–514.
[30] I.P. Sugár, E. Michonova-Alexova, P. Lee-Gau Chong, Geometrical Properties of Gel and Fluid Clusters in DMPC/DSPC Bilayers: Monte Carlo Simulation Approach Using a Two-State Model, Biophys. J. 81 (2001) 2425–2441.
[31] S.G. Brush, History of the Lenz-Ising Model, Rev. Mod. Phys. 39 (4) (1967) 883–893.
[32] P.F. Almeida, How to Determine Lipid Interactions in Membranes from Experiment Through the Ising Model, Langmuir 35 (1) (2019) 21–40.
[33] Q. Fei, D. Kent, W. Botello-Smith, F. Nur, S. Nur, A. Alsamarah, P. Chatterjee, M. Lambros, Y. Luo, Molecular Mechanism of Resveratrol's Lipid Membrane Protection, Sci. Rep. 8 (2018) 1587.
[34] R.G. Woolford, The Electrolysis Of ω-Bromocarboxylic Acids, Can. J. Chem. 40 (9) (1962) 1846–1850.
[35] T. Silva, B. Claro, B.F.B. Silva, N. Vale, P. Gomes, M.S. Gomes, S.S. Funari, J. Teixeira, D. Uhríková, M. Bastos, Unravelling a Mechanism of Action for a Cecropin A-Melittin Hybrid Antimicrobial Peptide: The Induced Formation of Multilamellar Lipid Stacks, Langmuir 34 (2018) 2158–2170.
[36] K. Vanommeslaeghe, E. Hatcher, C. Acharya, S. Kundu, S. Zhong, J. Shim, E. Darian, O. Guvench, P. Lopes, I. Vorobyov, A.D. Mackerell Jr., CHARMM general force field: A force field for drug-like molecules compatible with the CHARMM all-atom additive biological force fields, J. Comput. Chem. 31 (2010) 671–690.
[37] W. Yu, X. He, K. Vanommeslaeghe, A.D. MacKerell, Extension of the CHARMM general force field to sulfonyl-containing compounds and its utility in biomolecular simulations, J. Comput. Chem. 33 (31) (2012) 2451–2468.
[38] K. Vanommeslaeghe, A.D. MacKerell, Automation of the CHARMM General Force Field (CGenFF) I: Bond Perception and Atom Typing, J. Chem. Inf. Model. 52 (12) (2012) 3144–3154.
[39] K. Vanommeslaeghe, E.P. Raman, A.D. MacKerell, Automation of the CHARMM General Force Field (CGenFF) II: Assignment of Bonded Parameters and Partial Atomic Charges, J. Chem. Inf. Model. 52 (2012) 3155–3168.
[40] S. Jo, T. Kim, V.G. Iyer, W. Im, CHARMM-GUI: A web-based graphical user interface for CHARMM, J. Comput. Chem. 29 (2008) 1859–1865.
[41] S. Jo, T. Kim, W. Im, A. Yuan, Automated Builder and Database of Protein/Membrane Complexes for Molecular Dynamics Simulations, PLoS ONE 2 (9) (2007) e880.
[42] S. Jo, J.B. Lim, J.B. Klauda, W. Im, CHARMM-GUI Membrane Builder for Mixed Bilayers and Its Application to Yeast Membranes, Biophys. J. 97 (1) (2009) 50–58.
[43] E.L. Wu, X.i. Cheng, S. Jo, H. Rui, K.C. Song, E.M. Dávila-Contreras, Y. Qi, J. Lee, V. Monje-Galvan, R.M. Venable, J.B. Klauda, W. Im, CHARMM-GUI Membrane Builder toward realistic biological membrane simulations, J. Comput. Chem. 35 (27) (2014) 1997–2004.
[44] J. Lee, X.i. Cheng, J.M. Swails, M.S. Yeom, P.K. Eastman, J.A. Lemkul, S. Wei, J. Buckner, J.C. Jeong, Y. Qi, S. Jo, V.S. Pande, D.A. Case, C.L. Brooks, A.D. MacKerell, J.B. Klauda, W. Im, CHARMM-GUI Input Generator for NAMD, GROMACS, AMBER, OpenMM, and CHARMM/OpenMM Simulations Using the CHARMM36 Additive Force Field, J. Chem. Theory Comput. 12 (1) (2016) 405–413.
[45] J. Lee, D.S. Patel, J. Ståhle, S.-J. Park, N.R. Kern, S. Kim, J. Lee, X.i. Cheng, M.A. Valvano, O. Holst, Y.A. Knirel, Y. Qi, S. Jo, J.B. Klauda, G. Widmalm, W. Im, CHARMM-GUI Membrane Builder for Complex Biological Membrane Simulations with Glycolipids and Lipoglycans, J. Chem. Theory Comput. 15 (1) (2019) 775–786.
[46] J. Lee, M. Hitzenberger, M. Rieger, N.R. Kern, M. Zacharias, W. Im, CHARMM-GUI supports the Amber force fields, J. Chem. Phys. 153 (2020) 035103.
[47] P. Mark, L. Nilsson, Structure and Dynamics of the TIP3P, SPC, and SPC/E Water Models at 298 K, J Phys Chem A. 105 (43) (2001) 9954–9960.
[48] A. Srivastava, A. Debnath, Hydration dynamics of a lipid membrane: Hydrogen bond networks and lipid-lipid associations, J. Chem. Phys. 148 (2018) 094901.
[49] M.J. Abraham, T. Murtola, R. Schulz, S. Páll, J.C. Smith, B. Hess, E. Lindahl, GROMACS: High performance molecular simulations through multi-level parallelism from laptops to supercomputers, SoftwareX. 1–2 (2015) 19–25.
[50] S. Páll, B. Hess, A flexible algorithm for calculating pair interactions on SIMD architectures, Comput. Phys. Commun. 184 (12) (2013) 2641–2650.
[51] T. Darden, D. York, L. Pedersen, Particle mesh Ewald: An N·log(N) method for Ewald sums in large systems, J. Chem. Phys. 98 (1993) 10089–10092.
[52] B. Hess, H. Bekker, H.J.C. Berendsen, J.G.E.M. Fraaije, LINCS: A linear constraint solver for molecular simulations, J. Comput. Chem. 18 (1997) 1463–1472.
[53] H.J.C. Berendsen, J.P.M. Postma, W.F. van Gunsteren, A. DiNola, J.R. Haak, Molecular dynamics with coupling to an external bath, J. Chem. Phys. 81 (8) (1984) 3684–3690.
[54] S. Nosé, A molecular dynamics method for simulations in the canonical ensemble, Mol. Phys. 52 (2) (1984) 255–268.
[55] W.G. Hoover, Canonical dynamics: Equilibrium phase-space distributions, Phys. Rev. A. 31 (1985) 1695–1697.
[56] M. Parrinello, A. Rahman, Polymorphic transitions in single crystals: A new molecular dynamics method, J. Appl. Phys. 52 (1981) 7182–7190.
[57] N. Yellin, I.W. Levin, Hydrocarbon chain trans-gauche isomerization in phospholipid bilayer gel assemblies, Biochemistry 16 (4) (1977) 642–647.
[58] H. Heerklotz, H. Binder, G. Lantzsch, G. Klose, A. Blume, Lipid/Detergent Interaction Thermodynamics as a Function of Molecular Shape, J. Phys. Chem. B 101 (4) (1997) 639–645.
[59] J. Sabín, G. Prieto, J. Estelrich, F. Sarmiento, M. Costas, Insertion of semifluorinated diblocks on DMPC and DPPC liposomes. Influence on the gel and liquid states of the bilayer, J. Colloid Interface Sci. 348 (2) (2010) 388–392.
[60] J.E. McMurry, Organic Chemistry, 8th ed., Brooks/Cole Publishing Co., Canada, 2012.
[61] W. Chen, F. Duša, J. Witos, S. Ruokonen, S.K. Wiedmer, Determination of the Main Phase Transition Temperature of Phospholipids by Nanoplasmonic Sensing, Sci. Rep. 8 (2018) 14815.
[62] R.L. Biltonen, D. Lichtenberg, The use of differential scanning calorimetry as a tool to characterize liposome preparations, Chem. Phys. Lipids. 64 (1-3) (1993) 129–142.
[63] C. Arnulphi, J. Sot, M. García-Pacios, J.R. Arrondo, A. Alonso, F.M. Goñi, Triton X-100 Partitioning into Sphingomyelin Bilayers at Subsolubilizing Detergent Concentrations: Effect of Lipid Phase and a Comparison with Dipalmitoylphosphatidylcholine, Biophys. J. 93 (2007) 3504–3514.
[64] S. Leekumjorn, A.K. Sum, Molecular studies of the gel to liquid-crystalline phase transition for fully hydrated DPPC and DPPE bilayers, Biochim. Biophys. Acta (BBA) – Biomembr. 1768 (2) (2007) 354–365.
[65] A. Debnath, F.M. Thakkar, P.K. Maiti, V. Kumaran, K.G. Ayappa, Laterally structured ripple and square phases with one and two dimensional thickness modulations in a model bilayer system, Soft Matter 10 (38) (2014) 7630–7637.
[66] S.-S. Qin, Z.-W. Yu, Y.-X. Yu, Structural Characterization on the Gel to Liquid-Crystal Phase Transition of Fully Hydrated DSPC and DSPE Bilayers, J. Phys. Chem. B 113 (23) (2009) 8114–8123.
[67] K. Uppulury, P.S. Coppock, J.T. Kindt, Molecular Simulation of the DPPE Lipid Bilayer Gel Phase: Coupling between Molecular Packing Order and Tail Tilt Angle, J. Phys. Chem. B 119 (2015) 8725–8733.
[68] P.D. Dobson, D.B. Kell, Carrier-mediated cellular uptake of pharmaceutical drugs: an exception or the rule?, Nat Rev. Drug Discovery 7 (3) (2008) 205–220.
[69] W. Pezeshkian, H. Khandelia, D. Marsh, Lipid Configurations from Molecular Dynamics Simulations, Biophys. J. 114 (8) (2018) 1895–1907.